Available online at www.sciencedirect.com

ScienceDirect

Ceramics International 39 (2013) 9405–9414

CERAMICS INTERNATIONAL

www.elsevier.com/locate/ceramint

A facile and "green-chemistry" method to synthesize pure and Nd-doped $Y_3Al_5O_{12}$ nanopowders at low-temperatures

Esmeralda Mendoza-Mendoza[a], Sagrario M. Montemayor[b], Mirosław Maczka[c], Łukasz Marciniak[c], Antonio F. Fuentes[a,*]

[a]Cinvestav Unidad Saltillo, Apartado Postal 663, 25000 Saltillo, Coahuila, Mexico
[b]Facultad de Ciencias Químicas, Universidad Autónoma de Coahuila, Bulevar V. Carranza s/n, 25280 Saltillo, Coahuila, Mexico
[c]Institute of Low Temperature and Structure Research, Polish Academy of Sciences, P.O. Box 1410, Wrocław 2, Poland

Received 22 February 2013; received in revised form 5 May 2013; accepted 5 May 2013
Available online 23 May 2013

Abstract

This contribution presents a simple and cost-effective route for the low-temperature and large-scale production of $Y_3Al_5O_{12}$ (yttrium aluminum garnet YAG) nanopowders. The proposed methodology combines a mechanically assisted metathesis reaction and the benefits of molten salts as reaction media. An appropriate mixture of hydrated metal nitrates was mechanically blended with NaOH to induce a metathesis reaction and obtain a precursor material. Spherical-like nanometric particles (< 30 nm) of pure as well as Nd-doped YAG were obtained after short firing of this precursor at temperatures ≤ 500 °C. Complete conversion to the target material was achieved when adding $NaNO_2$ to the reaction mixture. Different techniques were used to follow the process and characterize the reaction products.

Keywords: Molten salts synthesis; Metathesis; Garnet; $Y_3Al_5O_{12}$; Nanoparticles

1. Introduction

As most Al_2O_3-based oxides, garnet-type yttrium aluminate $Y_3Al_5O_{12}$ (YAG) presents a remarkable combination of thermal, optical and mechanical properties. Thus, YAG shows high chemical and thermal stability, low creep rate and good mechanical properties at high temperatures; furthermore, it is also optically isotropic and transparent from below 300 nm to above 4 μm. Accordingly, YAG has been extensively used over the last fifty years in a broad variety of applications in the fields of optics and electronics. In particular, doped with trivalent laser activator rare-earth ions such as Nd^{3+}, Eu^{3+} or Er^{3+}, YAG is undoubtedly the most popular host medium for high power continuous and Q-switched operating solid-state lasers. Single-crystalline and thus, defect-free ceramics were initially required for these applications. However, the slow growth rate of YAG single crystals and their rather limited doping possibilities because of concentration gradients stimulated intense research activity in chemical processing and sintering of polycrystalline powders; hence, advances achieved in recent years [1–4] have allowed the manufacture of transparent polycrystalline ceramics with similar or even better properties than single crystals [5]. This contribution adds up to this effort by presenting a simple, cost-effective and scalable "green chemistry" route for preparing pure and doped nanocrystalline YAG powders at very low temperatures.

At least three stoichiometric compounds exist in the Y_2O_3–Al_2O_3 phase diagram, i.e. $Y_3Al_5O_{12}$, $YAlO_3$ and $Y_4Al_2O_9$, with the first one being by far the most stable under equilibrium conditions. Some controversy have persisted long on the formation and thermal stability of the remaining two phases [6–9]; however, they are frequently found as stubborn impurities when synthesizing bulk YAG by different methods. In particular, $YAlO_3$ seems to form readily from almost any Y_2O_3:Al_2O_3 mixed composition although its stability decreases considerably at high temperatures. Hence, repeated grinding and long firing cycles above 1600 °C are needed in order to ensure single phase YAG powders. Several low-temperature and wet-chemical methods such as sol–gel, [10,11] co-precipitation [12,13] and self-propagating combustion reactions

*Corresponding author. Tel.: +52 844 438 9600; fax: +52 844 438 9610.
E-mail addresses: fuentesaf@live.com, antonio.fernandez@cinvestav.edu.mx (A.F. Fuentes).

0272-8842/$ - see front matter © 2013 Elsevier Ltd and Techna Group S.r.l. All rights reserved.
http://dx.doi.org/10.1016/j.ceramint.2013.05.057

[14,15] have successfully reduced the synthesis temperature to typically, by the 800–1200 °C interval. All these methods have their own merits but they are in general time consuming, not suitable for producing large batches and/or use expensive and harmful precursors and solvents. Therefore, identifying and developing low-waste and energy efficient procedures capable of providing the necessary volume of bulk YAG powders in an economically viable manner, is still of interest. In this work, a synergetic approach previously used in this group to prepare pure and doped nanocrystalline $LaAlO_3$ powders at very low temperatures [16–19], has been adapted for the preparation of YAG nanoparticles. The procedure which combines a metathesis reaction and molten alkali metal nitrates as a reaction media, yields Al_2O_3-based oxides at remarkably low temperatures.

Ionic molten salts are considered as a promising alternative in materials science to conventional solvents with great potential for the "green" synthesis of many advanced ceramics. Free from the limitations of slow diffusion kinetics in the solid state, reaction times in molten salt synthesis (MSS) are considerably reduced as compared to the traditional ceramic method. Moreover, the materials of interest are commonly obtained as homogeneous and loosely agglomerated nanoparticles of high specific surface area. Therefore, lower processing temperatures are usually needed to achieve specific structural and/or microstructural characteristics. When targeting multicomponent oxides, MSS is usually carried out by blending the appropriate inorganic precursor salts with an excess of the desired flux and firing the mixture above the latter melting point [20–25]. Therefore, finding the right flux and/or precursor chemicals is crucial in determining the success of this processing technique. Alkali metal nitrates ANO_3 (A=Li, Na or K) are widely considered ideal fluxes for MSS because of their low cost, low melting points (below 340 °C) and thermal stability over a wide liquid temperature window (~500 °C) [21]; in addition, they show high water solubility and can be easily removed by a simple washing step. According to the Lux–Flood (L–F) formalism, molten ANO_3 nitrates are considered as oxide ion donors [26] and thus, behave as a basic reaction media toward many chemical species which will commonly either precipitate as an oxide or remain in the melt as soluble oxy-ions. Molten alkali metal nitrites ANO_2 are a greater source of oxide ions than nitrates and thus, are frequently used in MSS to increase the basicity of the melt and favor reactivity [27]. Additionally, $NaNO_3$/$NaNO_2$ mixtures present lower melting points than the two single salts and provide a larger temperature window to perform chemical reactions; thus, whereas the melting point of the $NaNO_3$:$NaNO_2$ eutectic (1:1 mol fraction) is 230 °C, those of single $NaNO_3$ and $NaNO_2$ increase to 303 °C and 283 °C respectively [28]. In this work, $NaNO_3$ and $NaNO_3$/$NaNO_2$ mixtures were analyzed as fluxes for the MSS of pure and Nd-doped YAG powders using different chemicals as metal sources.

2. Experimental procedure

The experimental metathesis/molten salts hybrid processing protocol followed in the present work is similar to that described previously [e.g. see [17]] consisting basically of three simple steps: (i) a mechanically induced metathesis reaction, (ii) short firing at low temperatures and (iii) washing with distilled water. The procedure does not involve organic solvents or special equipment and can be completed in a short period of time. Two different reaction temperatures (350 and 500 °C) were tested during this investigation. A typical experiment would consist of:

(i) Milling

Commercially available hydrated yttrium and aluminum nitrates ($Y(NO_3)_3 \cdot 4H_2O$ and $Al(NO_3)_3 \cdot 9H_2O$, *Sigma-Aldrich*, *St. Louis*, *United States*) were weighed out as required by stoichiometry (Y:Al molar ratio = 3:5) and mixed together with NaOH. The amount of reactants was salt-balanced according to the hypothetical reaction presented below (NaOH:(Al+Y) molar ratio = 3:1) such that there was no sodium hydroxide or nitrates excess

$$5[Al(NO_3)_3 \cdot 9H_2O]+3[Y(NO_3)_3 \cdot 4H_2O]+24NaOH \rightarrow Y_3Al_5O_{12}+24NaNO_3+69H_2O$$

The reaction mixture was transferred to yttria partially stabilized zirconia containers (5.2 wt% Y_2O_3) together with 20 mm diameter balls of the same material as grinding media; milling was carried out for 30 min in a Restch PM400 planetary ball mill (*Retsch GmbH*, Haan, Germany) using a rotating disc speed of 350 rpm and a balls-to-powder mass ratio of 10:1. The material obtained after this step is called *"precursor"* and contains in-situ generated $NaNO_3$ which is used as reaction media for preparing polycrystalline YAG. When using sodium nitrite $NaNO_2$ (*Sigma-Aldrich*, *St. Louis*, *United States*), this chemical was incorporated into the reaction mixture (NaOH:$NaNO_2$ molar ratio = 3:1) before milling.

(ii) Firing

The as-prepared *precursor* material was dried for 1 h at 120 °C to reduce moisture and minimize violent gas evolution on melting, loaded into high alumina crucibles and heated in an electrical furnace (heating rate = 5 °C min^{-1}); samples were allowed to naturally cool inside the furnace.

(iii) Washing

The resulting solidified melt was washed several times with distilled water under vigorous stirring to remove the water soluble byproducts and the remaining solid was collected by centrifugation. This step was repeated until no traces of NO_3^- or NO_2^- ions were detected by FTIR spectroscopy. When preparing Nd-doped YAG samples, an appropriate amount of $Nd(NO_3)_3 \cdot 6H_2O$ (*Sigma-Aldrich*, *St. Louis*, *United States*) as required by stoichiometry was added before milling to the reaction mixture described above.

Additional experiments were carried out to test the feasibility of synthesizing YAG powders in molten nitrates/nitrites following the conventional MSS approach described previously. Thus, $NaNO_3$ or $NaNO_3$/$NaNO_2$ mixtures were directly blended with

high purity Y_2O_3 and Al_2O_3 (*Sigma-Aldrich*, *St. Louis*, *United States*) or $Y(NO_3)_3 \cdot 4H_2O$ and $Al(NO_3)_3 \cdot 9H_2O$ and fired at the same reaction temperatures (350 and 500 °C) for 3 h.

Different characterization techniques were used to follow the experimental procedure. Thus, phase identification was carried out by X-ray diffraction in an X'Pert PRO diffractometer (*PANanalytical B.V.*, *Almelo*, *Holland*) equipped with a linear PIXcel detector and using CuKα_1 radiation ($\lambda = 1.54056$ Å; measurement range $= 5^o \leq 2\theta \leq 140^o$; and step size $= 0.026^o$)

The thermal behavior of the as-prepared samples was examined in a Perkin-Elmer Pyris Diamond TG/DTA instrument (*Perkin-Elmer*, *Inc*, *Waltham*, *MS*, *United States*) by simultaneously recording the thermogravimetric and differential analysis curves using a typical sample size of 15 mg, a 5 °C/min heating rate and an air static atmosphere.

Particle size and morphology were analyzed using a Philips CM20 SuperTwin transmission electron microscope (*Philips Export B.V.*, *Eidhoven, Holland*) providing 0.24 nm resolution. Specimens for TEM were prepared by dispersing the samples in methanol with ultrasonic agitation and depositing a droplet of suspension on the surface of a microscope grid covered with carbon film.

Infrared spectra were measured (spectral resolution $= 2\ cm^{-1}$) using a Biorad 575C FT-IR spectrometer (*Bio-Rad Laboratories*, *Inc*, *Cambridge*, *MA*, *United States*) in KBr pellets for the 4000–400 cm^{-1} region and in Nujol suspensions for the 500–50 cm^{-1} region. Emission spectra were measured using a Renishaw InVia spectrometer (*Renishaw plc*, *Old Town Wotton-under-Edge, Gloucestershire*, *United Kingdom*) equipped with a confocal DM 2500 Leica optical microscope (*Leica Microsystems CMS GmbH*, *Wetzlar*, *Germany*), a thermoelectrically cooled Ren Cam CCD as a detector and a diode laser operating at 830 nm.

3. Results and discussion

3.1. Reactivity of Y(III) and Al(III) oxides and hydrated metal nitrates in molten nitrates/nitrites

Two different Y(III) and Al(III) sources (i.e. oxides and hydrated nitrates) were tested for the synthesis of YAG powders in molten nitrate/nitrite using the conventional MSS approach. Fig. 1(a) presents the XRD pattern collected after firing at 350 °C for 3 h a mixture of both oxides (3:5 M ratio) and commercially available $NaNO_3$. As shown in this figure, the only reflections observed are those characteristic of the starting chemicals; thus, Y and Al oxides does not show any reactivity in molten sodium nitrate.

Fig. 1(b) shows the XRD pattern obtained after firing a mixture of hydrated metal nitrates and $NaNO_3$ at 350 °C for 3 h. $NaNO_2$ was even added this time to increase reactivity. However, the only crystalline product clearly identified is $NaNO_3$ (JCPDS-ICCD card no. 36-1474) although there is in addition a group of low intensity reflections appearing between 15° and 22° (2θ). While this group of reflections could not be assigned with certainty to any known chemical species, they definitely do not belong to YAG or to any other known Al(III) and Y(III) mixed oxide.

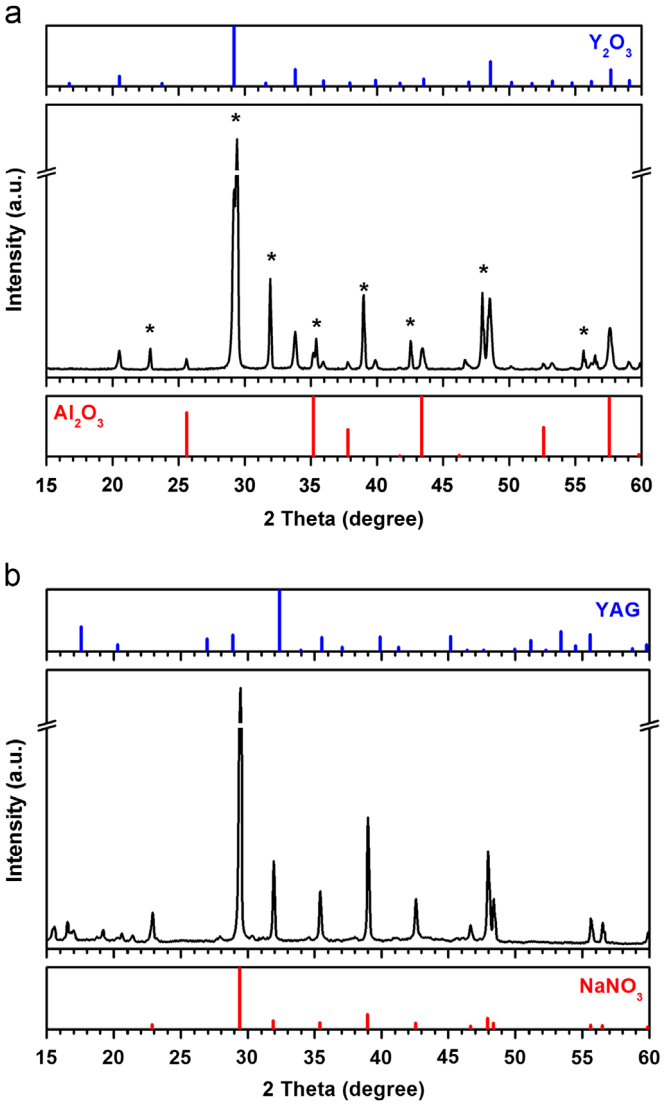

Fig. 1. (a) XRD patterns of a mixture of Y_2O_3, Al_2O_3 and $NaNO_3$ after firing for 3 h at 350 °C. Reflections marked with asterisks are those characteristic of $NaNO_3$ whereas top and bottom diagrams show the Bragg reflections of both starting oxides. (b) XRD patterns of a mixture of hydrated yttrium and aluminum nitrates and $NaNO_3$/$NaNO_2$ after firing for 3 h at 350 °C; top and bottom diagrams show the Bragg reflections of $Y_3Al_5O_{12}$ and $NaNO_3$ respectively.

Increasing the reaction temperature to 500 °C has no effect in either case and the XRD patterns collected (not shown) are very similar to those presented in Fig. 1. Therefore, neither oxides nor hydrated metal nitrates are good precursor chemicals for the synthesis of YAG in molten nitrates/nitrites using the conventional MSS approach.

3.2. Effect of a metathesis reaction in the synthesis of bulk YAG in molten nitrates/nitrites

Fig. 2 shows the XRD analysis of a mixture of hydrated yttrium and aluminum nitrates and NaOH after the three steps identified in the Experimental section: i.e. milling (a), firing (b) and washing (c). As Fig. 2(a) shows, mechanical milling do trigger a metathesis reaction in the starting mixture revealed by

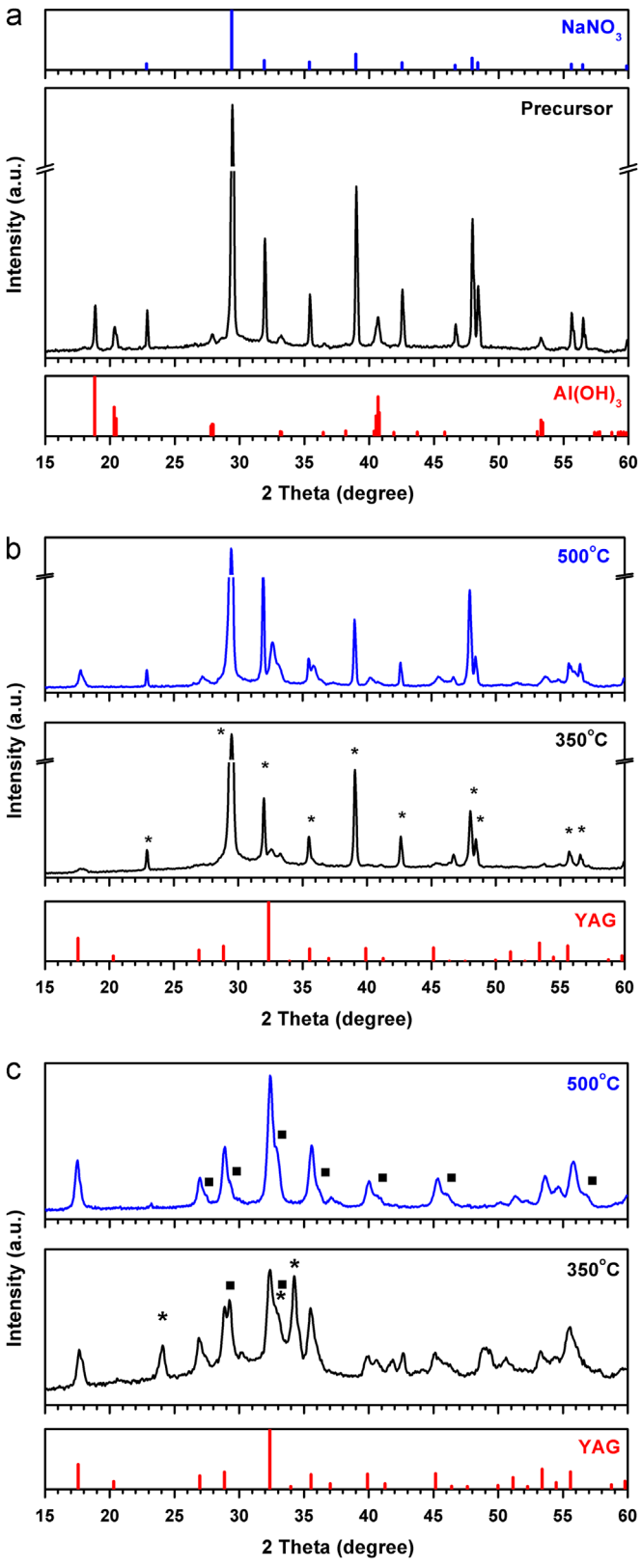

Fig. 2. XRD patterns of a mixture of $Y(NO_3)_3 \cdot 4H_2O$, $Al(NO_3)_3 \cdot 9H_2O$ and NaOH after milling (a), firing at 350 and 500 °C (b) and removing the water soluble byproduct in the latter (c). Top and bottom diagrams in (a) show the Bragg reflections of $NaNO_3$ and bayerite $Al(OH)_3$ whereas that depicted in (b) and (c) belongs to $Y_3Al_5O_{12}$. Reflections marked with an asterisk in (b) belong to $NaNO_3$. Reflections labeled with stars and solid squares in (c) belong to orthorhombic and cubic $YAlO_3$ respectively.

the presence of the characteristic reflections of $NaNO_3$; additionally, the main reflections of bayerite $Al(OH)_3$ are also evident (JCPDS-ICCD card no. 74-1119) such as those at 18.83° [Miller indexes = 001; relative intensity = 100%), 20.31° (110; 46%), 20.48 (020; 26%) and additional groups around 28° and 40° (2θ). The as-obtained *precursor* material was fired at 350 and 500 °C; as shown in Fig. 2(b), the XRD patterns collected confirm after this step the formation of the target material (JCPDS-ICDD card no. 33-0040): e.g. characteristic reflections at 18.09° [Miller indexes = 211; relative intensity = 27%), 27.79° (123; 19%) and 33.35° (024; 100%) (2θ). Intensity of the YAG reflections increases with increasing reaction temperature. However, some additional peaks are also observed close to those characteristic of YAG and toward higher 2θ angles as for example in 33° and 36° (2θ). These reflections are more evident in Fig. 2(c) which shows the XRD patterns of the same samples after removing the water soluble $NaNO_3$ flux; by comparison with the JCPDS-ICDD databank, it was possible to identify the presence of a different yttrium aluminum mixed oxides, $YAlO_3$. There are at least two perovskite-type $YAlO_3$ allotropic forms of orthorhombic and hexagonal symmetry reported in literature. In addition, a cubic "$YAlO_3$" phase with a garnet structure has been also observed when processing aluminum and yttrium mixtures using some specific powder methods: e.g. when firing at ~1000 °C amorphous precursors prepared by the simultaneous hydrolysis of Y(III) and Al(III) alkoxides [29,30] or electrochemically in molten $LiNO_3$ [31]. The garnet-type $Y_3Al_5O_{12}$ crystal framework is made up of corner-sharing AlO_4 tetrahedra and AlO_6 octahedra with yttrium atoms residing in dodecahedral interstices formed by such polyhedral network. Garnet-type $YAlO_3$ can be alternatively seen as an Al-poor YAG phase with half of the six-coordinated Al atoms replaced by yttrium and thus, might be formulated as $Y_3AlY(AlO_4)_3$ [30]. Interestingly, powders fired at 350 °C show the presence of both, orthorhombic and cubic forms of $YAlO_3$; the former is identified (JCPDS-ICDD card no. 33-0041) by its most intense reflection (Miller indexes = 121) at 34.27° (2θ) and by additional peaks at for example 23.98° (2θ) (101; 29%). Despite of overlapping reflections with YAG because of structural similarity, the presence of garnet-type $YAlO_3$ (JCPDS-ICDD card no. 38-0222) is inferred by the reflection appearing at 29.48° (2θ) (Miller indexes = 400; relative intensity = 30%) which belong neither to YAG nor to orthorhombic YAP. The sample also contains some amorphous phase denoted by a broad background between 25 and 40° (2θ). Increasing the reaction temperature to 500 °C prevents the formation of orthorhombic YAP but not of the cubic form. Nevertheless, their intensity is considerably smaller than in the sample obtained at 350 °C as is also the amount of amorphous phase.

Therefore, by introducing a metathesis reaction prior to the firing step it is possible to circumvent Y(III) and Al(III) low reactivity in molten nitrates and produce polycrystalline YAG at low temperatures; however, the target phase is obtained mixed with another garnet-type oxide with a stoichiometry close to $YAlO_3$.

It was decided then to analyze the effect of adding $NaNO_2$ (increase basicity) in the reaction outcome. Fig. 3 shows an XRD analysis of the evolution of a mixture of hydrated Y(III)

and Al(III) nitrates, NaOH and $NaNO_2$ after milling (a), firing (b) and washing with distilled water (c). As Fig. 3(a) shows, the presence of $NaNO_2$ does not inhibit the metathesis reaction as proved by the presence of $NaNO_3$ characteristic reflections besides those of $NaNO_2$ (JCPDS-ICDD card no. 87-1121). Yttrium seems to be present as amorphous species whereas aluminum is at least partially detected as bayerite $Al(OH)_3$ as denoted by the reflection showing at 18.89° (2θ) (Miller indexes = 001; relative intensity = 100%). However, the characteristic reflections of the latter are much weaker than in the XRD pattern shown in Fig. 2(a) and obtained when milling in the absence of $NaNO_2$. Firing the as-obtained precursor material at 350 or 500 °C produces YAG powders which can be isolated by washing with distilled water (Fig. 3(b) and (c)). According to XRD, no additional phases are observed with $NaNO_2$ reducing also the amount of amorphous phase present even at the lowest temperature. Therefore, the synergetic metathesis/molten salts approach allows to obtain YAG in $NaNO_3$/$NaNO_2$ at remarkably low temperatures.

3.3. Synthesis of Nd-doped YAG in molten $NaNO_3$/$NaNO_2$ mixtures

The proposed methodology was successfully tested for preparing Nd-doped YAG powders (0.5 and 1%) using hydrated neodymium nitrate as metal source. The experimental protocol used was the same as already described and the XRD patterns collected after completing the process did not show the presence of any additional phase but pure YAG.

3.4. Thermal analysis of some precursor materials

In order to gain some understanding about differences in reactivity, some Y(III) and Al(III) precursors were also analyzed using thermogravimetry and differential thermal analysis. Fig. 4 shows the thermal analysis curves obtained for different reaction mixtures selected as representatives of the series when subjected to the same heating/cooling program. Hydrated Y and Al nitrates (3:5 M ratio) are the metal sources in all cases; the main difference between samples is the flux used in the MSS step: commercially available $NaNO_3$ and $NaNO_2$ in (a) vs. in-situ generated $NaNO_3$ without and with added $NaNO_2$ in (b) and (c) respectively.

The first conclusion to be drawn from fig. 4 is that weight losses between room-temperature and 550 °C (left Y axis) are far more important in (a) than in (b) and (c). These differences are most likely due to the influence of mechanical milling on the water content of the reaction mixture as well as in the initial steps of the thermal decomposition of both hydrated metal nitrates. Although hydrated Y and Al nitrates are initially present in all three reaction mixtures, they are replaced in (b) and (c) during the mechanically induced metathesis reaction by different chemical species. The same differences are also evident in the DTA curves. Thus, the presence of $NaNO_3$ in any reaction mixture should produce two endothermic events at 261 and 298 °C with no associated weight losses belonging to a reversible polymorphic transformation (II-$NaNO_3$ → I-$NaNO_3$) and melting respectively [32]. The DTA curve of

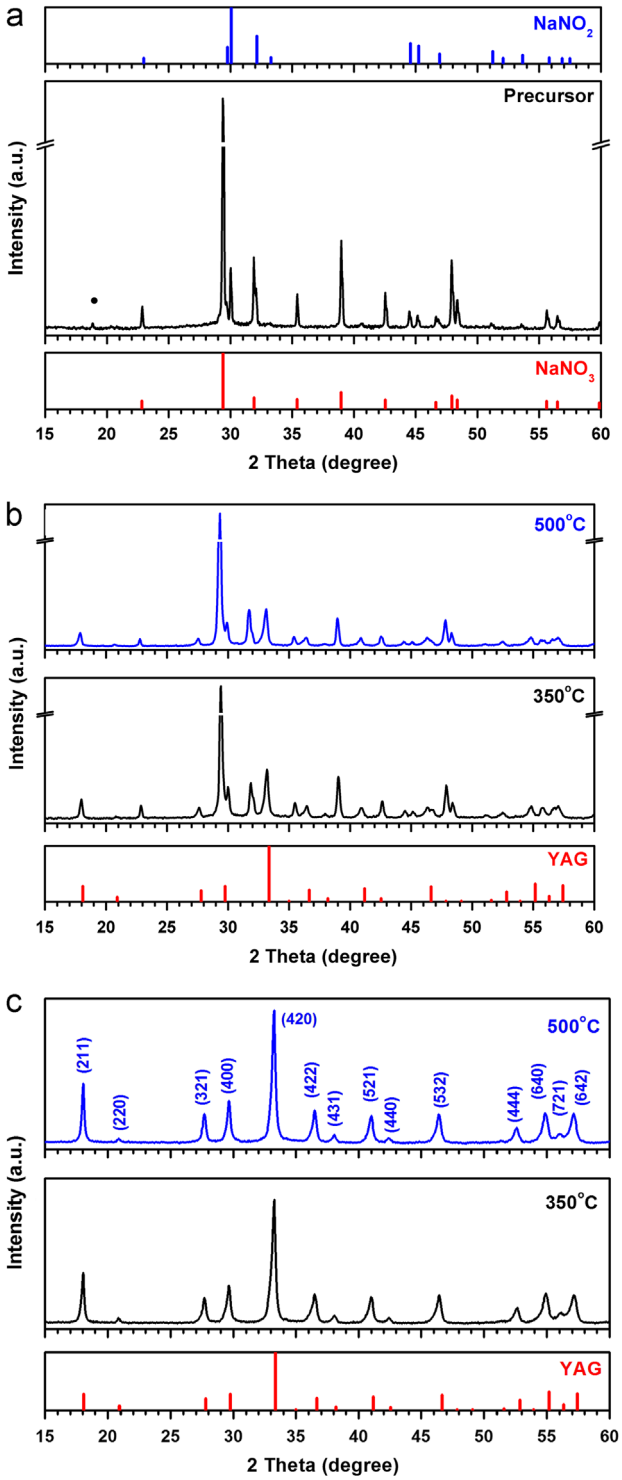

Fig. 3. XRD patterns of a mixture of $Y(NO_3)_3 \cdot 4H_2O$, $Al(NO_3)_3 \cdot 9H_2O$, NaOH and $NaNO_2$ after milling (a), firing at 350 and 500 °C (b) and removing the water soluble byproducts in the latter (c). Top and bottom diagrams in (a) show the Bragg reflections of $NaNO_3$ and $NaNO_3$ respectively whereas that depicted in (b) and (c) belongs to $Y_3Al_5O_{12}$. Reflection labeled in (a) belongs to bayerite $Al(OH)_3$.

pure $NaNO_2$ would also feature two endothermic events at temperatures close to 164 °C and 283 °C corresponding also to a phase transition and melting respectively [32]. A single eutectic has been proposed for the $NaNO_3$–$NaNO_2$ binary

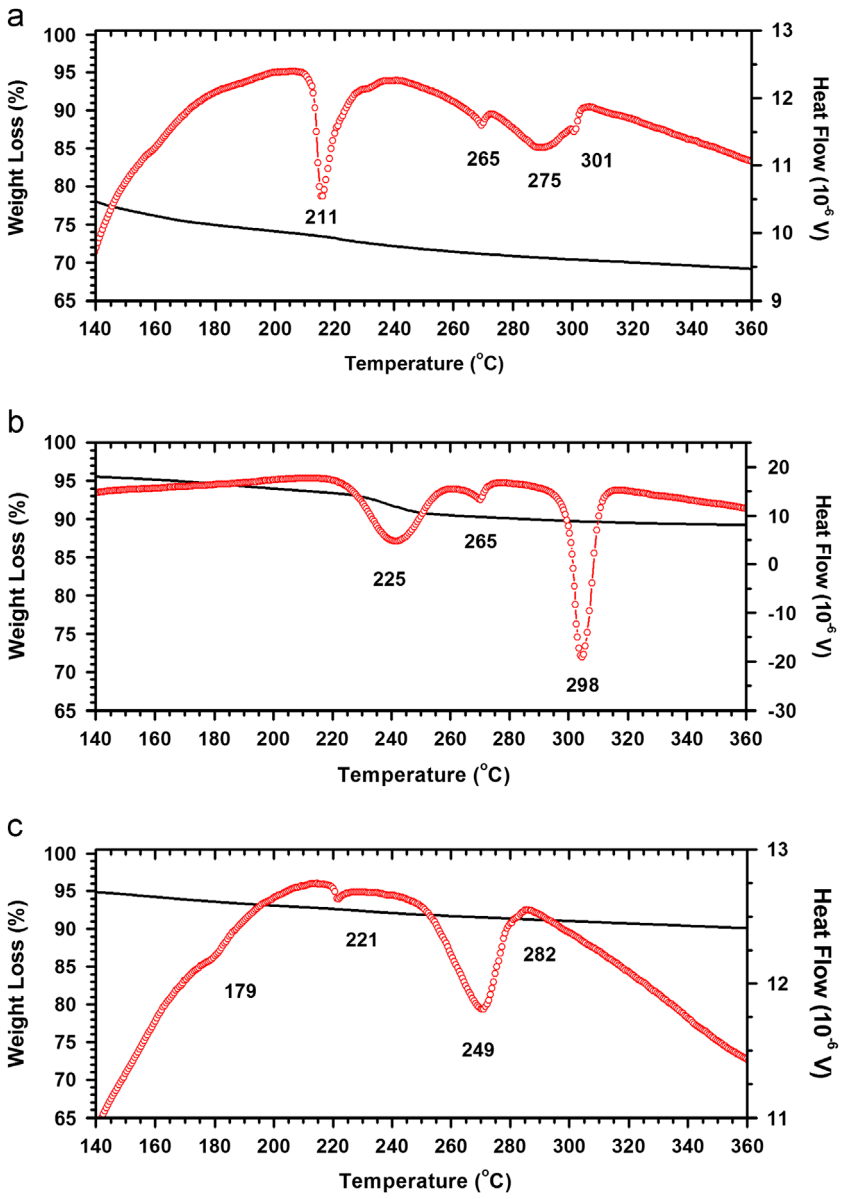

Fig. 4. Thermal analysis curves obtained for the following reaction mixtures: $Y(NO_3)_3 \cdot 4H_2O$, $Al(NO_3)_3 \cdot 9H_2O$, $NaNO_3$ and $NaNO_2$ (a), $Y(NO_3)_3 \cdot 4H_2O$, $Al(NO_3)_3 \cdot 9H_2O$ and NaOH (b) and $Y(NO_3)_3 \cdot 4H_2O$, $Al(NO_3)_3 \cdot 9H_2O$, NaOH and $NaNO_2$ (c).

phase diagram at the 1:1 mol fraction composition [28]; furthermore, the system also includes at 230 °C a horizontal solidus ranging from 0.25 to 0.80 mol fraction of $NaNO_3$ and two subsolidus transitions close to 160 °C and 183 °C. Our reaction mixtures where $NaNO_3$ was generated through a metathesis reaction (Fig. 4(b) and (c)), present the events expected in each case; thus, 4(b) clearly shows both events characteristic of $NaNO_3$ (the starting mixture does not contain $NaNO_2$) whereas 4(c) display the main events expected for a $NaNO_3/NaNO_2$ eutectic mixture (e.g. melting event with an onset temperature of 249 °C). Surprisingly, the characteristic events of the eutectic mixture are not present in the reaction mixture prepared using commercially available $NaNO_3$ and $NaNO_2$; instead, there is an important endothermic event without associated weight loss taking place at a temperature close to 211 °C and three minor ones at 265, 275 and 301 °C (a). Whereas the latter are probably due to $NaNO_3$ polymorphic transformation and melting (265 and 301 °C) and $NaNO_2$ melting (275 °C), the origin of the first one is uncertain. In a previous work published by this group and devoted to the synthesis of perovskite-type $LaAlO_3$ using a similar procedure to the one described here [16], a double nitrate $Na_2La(NO_3)_5 \cdot H_2O$ was identified as responsible for inhibiting the formation of the target material when using commercially available $NaNO_3$ as flux; such double nitrate was formed at low temperature by a chemical reaction between La and Na nitrates and had enough stability to hinder the formation of the target $LaAlO_3$ oxide. Although no yttrium and sodium double nitrate has been found in literature, the formation of a reaction product involving yttrium nitrate and either $NaNO_3$ or $NaNO_2$ would also explain the absence of events related to the $NaNO_3$–$NaNO_2$ eutectic in 4(a) as well as

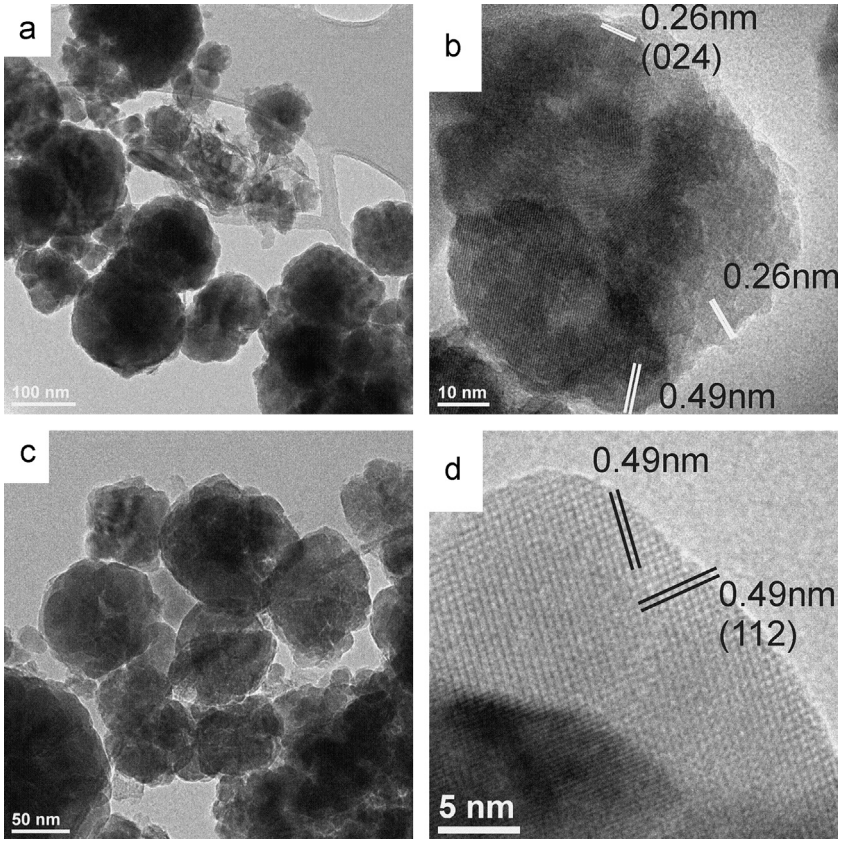

Fig. 5. TEM and HRTEM images of YAG powders prepared at 350 °C (a, b) and 500 °C (c, d).

the absence of $NaNO_2$ characteristic reflections in 1(b) since they would be mostly consumed by such reaction. The formation of such compound might account also for the group of reflections found in Fig. 1 (b) together with those of $NaNO_3$. Additional studies are currently underway to verify such possibility.

3.5. Size, morphology and formation mechanism of YAG crystallites in $NaNO_3$/$NaNO_2$

Pure and Nd-doped YAG powders prepared in $NaNO_3$/$NaNO_2$ were selected for further characterization and results are shown in the following sections. First of all, particle size was estimated by using XRD data and Scherrer's formula $D=K\lambda/\beta \cos \Theta$, where D is the mean crystallite size along the [hkl] direction, λ is the wavelength of the incident X-ray beam (in our study $\lambda=1.54056$ Å), β is broadening of the diffraction line (in radians), Θ is the angle of diffraction, and the Scherrer constant K is conventionally set to 1.0 [33,34]. Using the broadening of the (112) line, a mean crystallite size of 26.9 nm was calculated for the YAG samples synthesized at 350 °C and 500 °C; a similar crystallite size was found for the Nd-doped samples: 27.8 nm for YAG-0.5% Nd^{3+} and 29.8 nm for YAG-1% Nd^{3+}. Therefore, these results show that the crystallite size of the as-prepared YAG powders does not depend upon the reaction temperature or doping.

Further information on size and morphology of the synthesized crystallites was obtained by using transmission electron microscopy (TEM) with some representative micrographs presented in Fig. 5. Thus, Fig. 5(a) shows that the powder synthesized at 350 °C is composed of spherical-like particles with various sizes (~50–180 nm). However, high-resolution TEM (HRTEM) images shown in Fig. 5(b) show particles to be really composed of smaller regions with clear lattice fringes. Therefore, as-prepared YAG particles are well crystallized polydomains. The lattice fringe spacings in Fig. 5(b) are about 2.6 and 4.9 Å which correspond well with the separation between the (024) and (112) planes of cubic YAG, respectively. Fig. 5(a) also indicates that an additional amorphous phase (absence of lattice fringes) is also present. When the reaction temperature increases to 500 °C, the size of the spherical-like particles also increases slightly whereas the amorphous phase disappears (see Fig. 5(c)). HRTEM image shows very clear lattice fringes (see Fig. 5(d)) indicating the highly crystalline nature of the as-prepared YAG particles.

As for the formation reaction mechanism and depending on the difference in dissolution rates between reactants, there are two leading paths defining multicomponent phase formation in a liquid molten salt: *"dissolution–precipitation"* and *"template formation"*. Hence, the formation of a reaction product would take place through the first when both reactants present similar solubilities: i.e. the target material will precipitate during

cooling after the liquid flux becomes oversaturated. On the other hand, when dissolution rates are very different the reaction would follow the *"template formation"* mechanism: i.e. the more soluble reactant would dissolve in the flux, diffuse and react at the surface of the less soluble component to give a mixed compound. The first mechanism is thought to be the dominant in molten nitrates [35] and thus, responsible for YAG formation in molten $NaNO_3$–$NaNO_2$.

3.6. IR spectra of the obtained pure and Nd-doped YAG powders

YAG crystallizes in the cubic structure *Ia3d* (O_h^{10}) with eight formula units in the primitive cell. For the O_h^{10} structure of YAG, group theory predicts $3A_{1g}+5A_{2g}+8E_g+14F_{1g}+14F_{2g}+5A_{1u}+5A_{2u}+10E_u+17F_{1u}+16F_{2u}$ Brillouin zone center optic modes [36,37]. The A_{1g}, E_g and F_{2g} modes are Raman-active and F_{1u} modes are IR active. Therefore, there should be 17 IR bands for the *Ia3d* structure.

The IR spectra of YAG and YAG: Nd^{3+} samples are presented in Fig. 6. The spectrum of the YAG sample prepared at 350 °C shows bands at 168, 216, 295, 325, 368, 395, 485, 504, 563, 693, 722 and 786 cm^{-1}. IR spectra of the sample prepared at 500 °C as well as the YAG: Nd^{3+} samples show very similar bands which correspond well to the most intense IR bands reported for bulk and nanocrystalline YAG [34,35]. This result suggests high purity of the obtained YAG and YAG:Nd^{3+} samples. However, closer inspection of the spectra shows that the 368 cm^{-1} band observed for the samples prepared at 350 °C, shifts to higher wave numbers for the sample prepared at 500 °C, i.e. to 374 cm^{-1}. Moreover, its intensity significantly decreases. These effects cannot be attributed to any change of the crystallites size since according to our X-ray diffraction studies the crystallite size does not change. Therefore, it might be assumed that the amorphous phase detected by TEM in the sample prepared at 350 °C is also responsible for the 368 cm^{-1} band observed here; the presence and intensity of this band makes more complicated observing the 374 cm^{-1} band characteristic of the YAG phase due to overlapping. When the synthesis temperature increases to 500 °C, the band related to the amorphous material disappears making that related to YAG much more evident. As discussed above, our *precursor* contains a small amount of bayerite $Al(OH)_3$. Sato showed that bayerite decomposes partially into γ-AlOOH (boehmite) at 225 °C and then into γ-AlOOH and η-Al_2O_3 at 275 °C [38]. Far-IR study of boehmite showed that this material should have a medium intensity band at 326 cm^{-1} and a strong band at 366 cm^{-1} [39]. Although the first one would be overlapped by the broad and intense band of YAG observed at 325 cm^{-1}, the later agrees very well with the band observed in our specta at 368 cm^{-1}. This result suggests that samples synthesized at 350 °C contain amorphous γ-AlOOH as an impurity phase. Thus, our IR spectra are consistent with TEM and XRD data, and show that nanocrystalline YAG and YAG:Nd^{3+} are formed already at 350 °C but these samples also contain γ-AlOOH impurity phase.

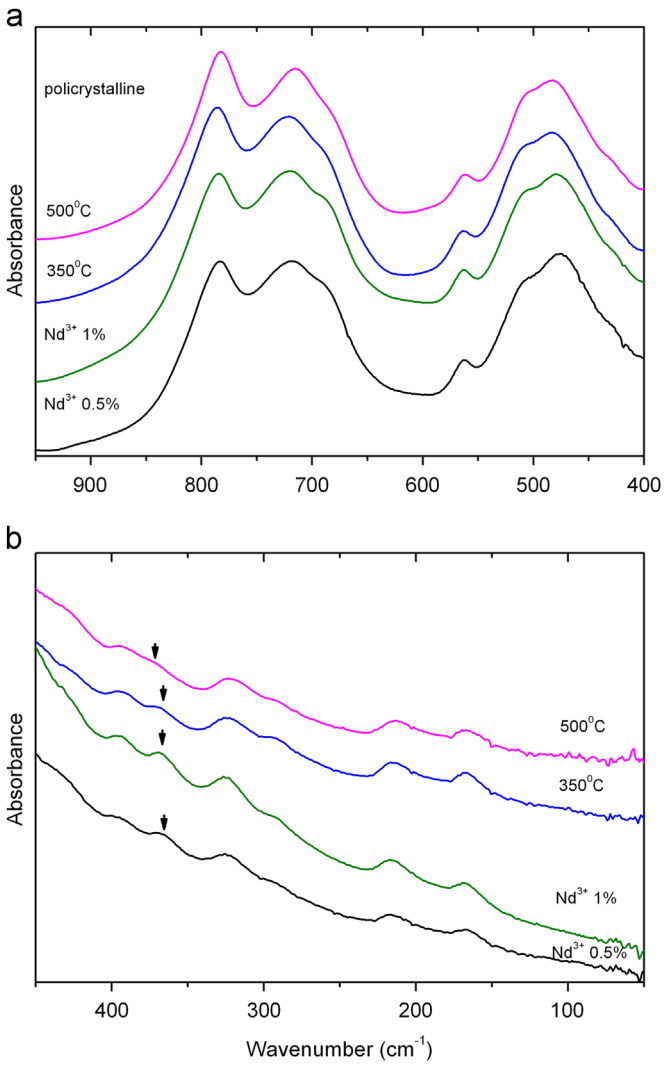

Fig. 6. IR spectra of YAG samples prepared at 350 °C and 500 °C as well as YAG: Nd^{3+} samples prepared at 350 °C in (a) the mid-IR and (b) far-IR region. Arrows indicate the 368 cm^{-1} and 374 cm^{-1} bands that corresponds to the impurity phase and YAG phase, respectively.

3.7. Emission spectra

Fig. 7 shows the emission spectra of YAG:0.5% Nd^{3+} and YAG:1% Nd^{3+} samples prepared at 350 °C associated with the $^4F_{3/2} \rightarrow {}^4I_{9/2}$ transition. For the comparison sake, the emission spectrum of single crystalline YAG:0.9% Nd^{3+} is also presented. This figure shows very clearly that almost all emission bands of our nanocrystalline samples originate from emission of YAG phase. This result proves that Nd^{3+} is successfully incorporated in the YAG structure even at this very low temperature. However, the observed emission is much weaker. Comparison of integral intensity shows that the emission intensity of our YAG:0.5 Nd^{3+} and YAG:1% Nd^{3+} nanopowders is about 53 and 120 times weaker, respectively, than that of the YAG:0.9 Nd^{3+} single crystal. Strong decrease of emission intensity was observed previously for nanocrystalline YAG:Nd^{3+} and attributed to the presence of large amount of hydroxyl groups on the nanocrystals surface [40,41]. Fig. 7

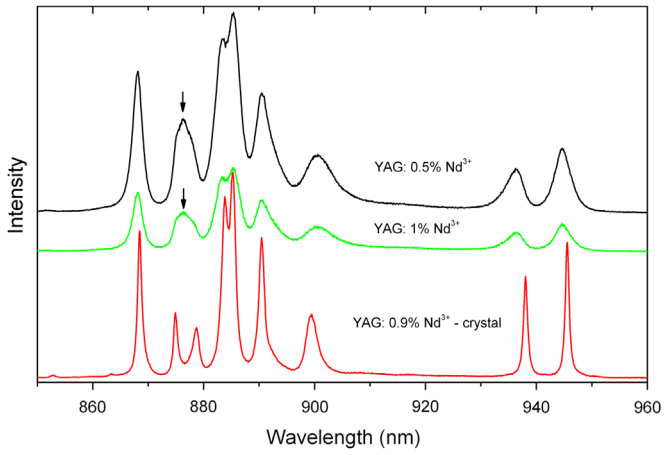

Fig. 7. The emission spectra of YAG: Nd^{3+} samples prepared at 350 °C under 830 nm excitation (laser power 30 mW). For the comparison sake, the emission spectrum of YAG:0.9 Nd^{3+} single crystal is also presented (laser power 0.3 mW). Arrows indicate the 876.3 nm band not related to YAG emission.

also shows that emission bands of YAG: Nd^{3+} samples are much broader than the corresponding bands of the single crystal. This result can be attributed to small size of crystallites and presence of defects. Apart from the bands characteristic for YAG phase, an additional broad band is observed at 876.3 nm. Interestingly, similar but much broader band was observed by some other authors at about 877 nm for an amorphous precursor of $LaAlO_3$:Nd^{3+} [42]. Therefore, this additional broad band can be attributed to the presence of an amorphous fraction and/or to the presence of Nd^{3+} in low symmetry sites near defects or the surface of the nanocrystals.

4. Conclusions

Pure and Nd-doped YAG nanoparticles have been successfully obtained at very low temperatures using a synergetic metathesis/molten salts approach. The combination of these two simple powder processing methods allows to overcome Al(III) and Y(III) low reactivity in molten nitrates/nitrites and to obtain the YAG phase at temperatures ≤500 °C. As-prepared samples consist of loosely agglomerated particles with a crystallite size below 30 nm. The "green" approach presented here is simple, scalable and cost-effective and thus, compares favorably with existing and much more challenging methodologies.

Acknowledgments

SMM thanks CUMEX for financial support for this work through the program "Becas de Capacitación: Estancias Post-doctorales en el Extranjero".

References

[1] A. Ikesue, T. Kinoshita, K. Kamata, K. Yoshida, Fabrication and optical properties of high-performance polycrystalline Nd:YAG ceramics for solid-state lasers, Journal of the American Ceramic Society 78 (1995) 1033–1040.
[2] A. Ikesue, I. Furusato, K. Kamata, Fabrication of polycrystalline, transparent YAG ceramics by a solid-state reaction method, Journal of the American Ceramic Society 78 (1995) 225–228.
[3] A. Ikesue, K. Kamata, K. Yoshida, Effects of neodymium concentration on optical characteristics of polycrystalline Nd:YAG laser materials, Journal of the American Ceramic Society 79 (1996) 1921–1926.
[4] A. Ikesue, K. Kamata, K. Yoshida, Synthesis of Nd^{3+}, Cr^{3+}-codoped YAG ceramics for high-efficiency solid state lasers, Journal of the American Ceramic Society 78 (1995) 2545–2547.
[5] A. Ikesue, Y.L. Aung, Synthesis and performance of advanced ceramic lasers, Journal of the American Ceramic Society 89 (2006) 1936–1944.
[6] I. Warshaw, R. Roy, Stable and metastable equilibria in the systems Y_2O_3–Al_2O_3 and Gd_2O_3–Fe_2O_3, Journal of the American Ceramic Society 42 (1959) 434–438.
[7] J.S. Abell, I.R. Harris, B. Cockayne, B. Lent, An investigation of the phase stability in the Y_2O_3–Al_2O_3 system, Journal of Materials Science 9 (1974) 527–537.
[8] B. Cockayne, The uses and enigmas of the Al_2O_3–Y_2O_3 phase system, Journal of the Less Common Metals 114 (1985) 199–206.
[9] M. Medraj, R. Hammond, M.A. Parvez, R.A.L. Drew, W.T. Thompson, High temperature neutron diffraction study of the Al_2O_3–Y_2O_3 system, Journal of the European Ceramic Society 26 (2006) 3515–3524.
[10] R.P. Rao, Preparation and characterization of fine-grain yttrium-based phosphors by sol–gel process, Journal of the Electrochemical Society 189 (1996) 189–197.
[11] M.K. Cinibulk, Synthesis of yttrium aluminum garnet from a mixed-metal citrate precursor, Journal of the American Ceramic Society 83 (2000) 1276–1278.
[12] J.G. Li, T. Ikegami, J.H. Lee, T. Mori, Y. Yajima, Co-precipitation synthesis and sintering of yttrium aluminum garnet (YAG) powders: the effect of precipitant, Journal of the European Ceramic Society 20 (2000) 2395–2405.
[13] A.M. George, N.C. Mishra, M.S. Nagar, N.C. Jayadevan, Formation of YAG from coprecipitated yttrium aluminum hydroxides, Journal of Thermal Analysis 47 (1996) 1701–1708.
[14] N.J. Hess, G.D. Maupin, L.A. Chick, D.S. Sunberg, D.E. McCreedy, T.R. Amstrong, Synthesis and crystallization of yttrium–aluminum garnet and related compounds, Journal of Materials Science 29 (1994) 1873–1878.
[15] J. Li, Y. Pan, F. Qiu, Y. Wu, J. Guo, Nanostructured Nd:YAG powders via gel combustion: the influence of citrate-to-nitrate ratio, Ceramics International 34 (2008) 141–149.
[16] E. Mendoza-Mendoza, K.P. Padmasree, S.M. Montemayor, A.F. Fuentes, Molten salts synthesis and electrical properties of Sr- and/or Mg-doped perovskite-type $LaAlO_3$ powders, Journal of Materials Science 47 (2012) 6076–6085.
[17] E. Mendoza-Mendoza, S.M. Montemayor, J.I. Escalante-Garcia, A.F. Fuentes, A Green-chemistry approach to the synthesis of rare-earth aluminates: perovskite-type $LaAlO_3$ nanoparticles in molten nitrates, Journal of the American Ceramic Society 95 (2012) 1276–1283.
[18] M. Maczka, E. Mendoza-Mendoza, A.F. Fuentes, K. Lemański, P. Dereń, Low-temperature synthesis, luminescence and phonon properties of Er and/or Dy doped $LaAlO_3$ nanopowders, Journal of Solid State Chemistry 187 (2012) 249–257.
[19] M. Maczka, A. Bednarkiewicz, E. Mendoza-Mendoza, A.F. Fuentes, L. Kępiński, Optical properties of Eu and Er doped $LaAlO_3$ nanopowders prepared by low temperature method, Journal of Solid State Chemistry 194 (2012) 264–269.
[20] K.H. Yoon, Y.S. Cho, D.H. Kang, Molten salt synthesis of lead-based relaxors, Journal of Materials Science 33 (1998) 2977–2984.
[21] P. Afanasiev, C. Geantet, Synthesis of solid materials in molten nitrates, Coordination Chemistry Reviews (178–180) (1998) 1725–1752.
[22] H. Zhou, Y. Mao, S.S. Wong, Probing structure-parameter correlations in the molten salt synthesis of $BaZrO_3$ perovskite submicrometer-sized particles, Chemistry of Materials 19 (2007) 5238–5249.
[23] Z. Cai, X. Xing, L. Li, Y. Xu, Molten salt synthesis of lead lanthanum zirconate titanate powders, Journal of Alloys and Compounds 454 (2008) 466–470.

[24] Y. Mao, S. Banerjee, S.S. Wong, Large-scale synthesis of single-crystalline perovskite nanostructures, Journal of the American Chemical Society 125 (2003) 15718–15719.
[25] B. Roy, P.A. Fuierer, Molten salt synthesis of $Bi_4(V_{0.85}Co_{0.15})_2O_{11-\delta}$ (BICOVOX) ceramic powders, Journal of the American Ceramic Society 92 (2009) 520–523.
[26] B.L. Trémillon, Acid–base effects in molten electrolytes, in: G. Mamantov, R. Marassi (Eds.), Molten Salt Chemistry: An Introduction and Selected Applications, NATO ASI Series, D. Reidel Publishing Company, Dordrecht, Holland, 1987, pp. 279–303.
[27] D.H. Kerridge, Stabilisation of high oxidation states in basic molten salts, Thermochimica Acta 200 (1992) 379–386.
[28] R.W. Berg, D.H. Kerridge, P.H. Larsen, $NaNO_2$+$NaNO_3$ phase diagram: new data from DSC and Raman spectroscopy, Journal of Chemical and Engineering Data 51 (2006) 34–39.
[29] O. Yamaguchi, K. Takeoka, K. Hirota, H. Takano, A. Hayashida, Formation of alkoxy-derived yttrium aluminum oxides, Journal of Materials Science 27 (1992) 1261–1264.
[30] O. Yamaguchi, K. Matui, K. Shimizu, Formation of $YAlO_3$ with garnet structure, Ceramics International 11 (1985) 107–108.
[31] Z. Liu, J. Ma, Y. Sun, Z. Song, J. Fang, Y. Liu, Ch. Gao, J. Zhao, Low-temperature molten salt synthesis of $YAlO_3$ powders assisted by an electrochemical process, Ceramics International 36 (2010) 2003–2006.
[32] C.N.R. Rao, B. Prakash, M. Natarajan, Crystal structure transformations in inorganic nitrites, nitrates, and carbonates, The National Standard Reference Data System (NSRDS–NBS 53), National Bureau of Standards, U.S. Department of Commerce, Washington, 1975.
[33] S. Chattopadhyay, P. Ayyub, V.R. Palkar, M. Multani, Size-induced diffuse phase transition in the nanocrystalline ferroelectric $PbTiO_3$, Physical Review B 52 (1995) 13177–13183.
[34] J.M. Amigó, F.J. Serrano, M.A. Kojdecki, J. Bastida, V. Esteve, M.M. Reventós, F. Marti, X-ray diffraction microstructure analysis of mullite, quartz and corundum in porcelain insulators, Journal of the European Ceramic Society 25 (2005) 1479–1486.
[35] H. Al Raihani, B. Durand, F. Chassagneux, D.H. Kerridge, D. Inman, Zirconia formation by reaction of zirconium sulfate in molten alkali-metal nitrates or nitrites, Journal of Materials Chemistry 4 (1994) 1331–1336.
[36] A.M. Hofmeister, K.R. Campbell, Infrared spectroscopy of yttrium aluminum, yttrium gallium, and yttrium iron garnets, Journal of Applied Physics 72 (1992) 638–646.
[37] A. Lukowiak, R.J. Wiglusz, M. Maczka, P. Gluchowski, W. Strek, IR and Raman spectroscopy of YAG nanoceramics, Chemical Physics Letters 494 (2010) 279–283.
[38] T. Sato, Thermal decomposition of aluminum hydroxides, Journal of Thermal Analysis 32 (1987) 61–70.
[39] H.D. Ruan, R.L. Frost, J.T. Kloprogge, L. Duong, Far-infrared spectroscopy of alumina phases, Spectrochimica Acta A 58 (2002) 265–272.
[40] M. Pokhrel, N. Ray, G.A. Kumar, D.K. Sardar, Comparative studies of the spectroscopic properties of Nd^{3+}: YAG nanocrystals, transparent ceramic and single crystal, Optical Materials Express 2 (2012) 235–249.
[41] D. Hreniak, R. Fedyk, A. Bednarkiewicz, W. Stręk, W. Łojkowski, Luminescence properties of Nd:YAG nanoceramics prepared by low temperature high pressure sintering method, Optical Materials 29 (2007) 1244–1251.
[42] R. Pazik, G.A. Seisenbaeva, S. Gohil, R. Wiglusz, L. Kepiński, W. Stek, Simple and efficient synthesis of Nd:$LaAlO_3$ NIR nanophosphor from rare earth alkoxo-monoaluminates $Ln_2Al_2(OiPr)_{12}(iPrOH)_2$ single source precursor by Bradley reaction, Inorganic Chemistry 49 (2010) 2684–2691.